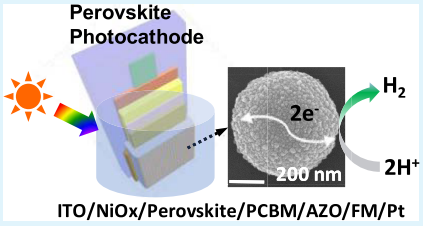
Triple-Cation-Based Perovskite Photocathodes with AZO Protective Layer for Hydrogen Production Applications

Shahab Ahmad,*[,†,‡] Aditya Sadhanala,[§,#] Robert L. Z. Hoye,[§,#] Virgil Andrei,[∥] Mohammad Hadi Modarres,[‡] Baodan Zhao,[§] Jan Rongé,[⊥] Richard Friend,[§] and Michael De Volder*[,‡]

[†]Centre for Nanoscience and Nanotechnology, Jamia Millia Islamia (A Central University), New Delhi 110025, India
[‡]Institute for Manufacturing, Department of Engineering, University of Cambridge, Cambridge CB3 0FS, United Kingdom
[§]Cavendish Laboratory, University of Cambridge, JJ Thomson Avenue, Cambridge CB3 0HE, United Kingdom
[∥]Department of Chemistry, University of Cambridge, Lensfield Road, Cambridge CB2 1EW, United Kingdom
[⊥]Centre for Surface Chemistry and Catalysis, KU Leuven, Leuven B-3001, Belgium

ABSTRACT: Metal halide perovskites are actively pursued as photoelectrodes to drive solar fuel synthesis. However, currently, these photocathodes suffer from limited stability in water, which hampers their practical application. Here, we report a high-performance solution-processable photocathode composed of cesium formamidinium methylammonium triple-cation lead halide perovskite protected by an Al-doped ZnO (AZO) layer combined with a Field's metal encapsulation. Careful selection of charge transport layers resulted in an improvement in photocurrent, fill factor, device stability and reproducibility. The dead pixels count reduced from 25 to 6% for the devices with an AZO layer, and in photocathodes with an AZO layer the photocurrent density increased by almost 20% to 14.3 mA cm^{-2}. In addition, we observed a 5-fold increase in the device lifetime for photocathodes with AZO, which reached up to 18 h before complete failure. Finally, the photocathodes are fabricated using low-cost and scalable methods, which have promise to become compatible with standard solution-based processes.



KEYWORDS: *metal halide perovskites, triple-cation, solar water splitting, proton reduction, photocathodes, water stability, metal oxide transport layers*

INTRODUCTION

The idea of converting water molecules into hydrogen and oxygen using sunlight has been around for almost a century[1−3] and received much attention after Fujishima and Honda demonstrated water splitting by photogenerated electron−hole pairs from UV-irradiated semiconducting particles.[4] Solar-powered water splitting results in so-called "solar fuels", which can provide a sustainable alternative for the existing fossil fuel-based technologies. While seemingly straightforward, this reaction is challenging, as it requires efficient generation, transport, and extraction of charge carriers, ions, and products upon the absorption of photons. Tremendous efforts have been invested in the design of photoelectrodes that drive these processes efficiently by engineering the band gap, charge transport, and catalyzing the reaction.[5−8] Semiconductors based on metal oxides ($BiVO_4$, Cu_2O, Fe_2O_3) as well as transition-metal disulfides (e.g., MoS_2) and selenides (e.g., WSe_2) absorb the solar spectrum with good efficiency and display long charge carrier diffusion lengths.[8−16]

Organo-lead halide perovskite-based crystalline semiconductors have gained substantial traction for photovoltaics and energy applications because of their high absorption coefficients, efficient electron−hole pair separation, cost efficiency, and long carrier diffusion lengths.[17−21] Further, they are straightforward to synthesize and can be processed using low-temperature methods owing to their tolerance to point defects. These properties make lead halide perovskites very attractive for solar water splitting applications. However, their limited lifetime and low photocurrent density, when submerged in water, limit their practical applications.[22−25] The first demonstration of a water-submerged $CH_3NH_3PbI_3$-based photoanode was reported in 2015 by Da et al., where a perovskite solar cell with a protective layer of evaporated Ni was employed to oxidize Na_2S as a hole scavenger. However, this device lost 80% of the initial photocurrent after 15 min of operation.[22] In 2016, Hoang et al. demonstrated the use of a carbon nanotube/polymer composite layer to protect the underlying perovskite layer from electrolyte molecules[23] and achieved 30 min of operation. In 2016, Crespo-Quesada et al. demonstrated a novel protection methodology where a low-

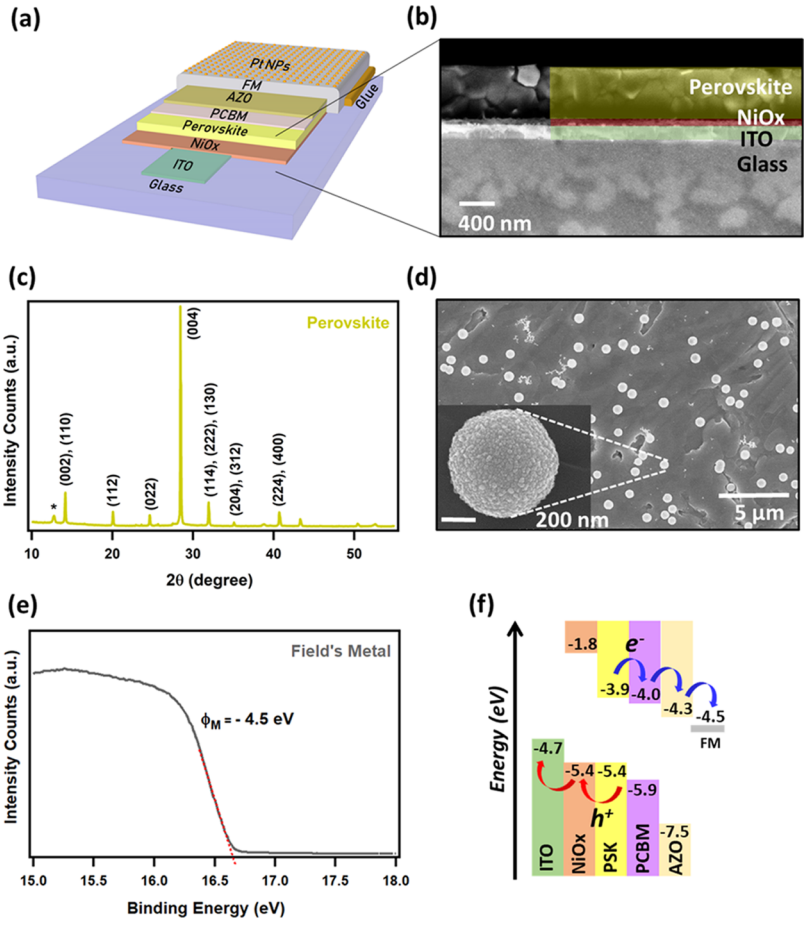


Figure 1. (a) Schematic representation of the perovskite photocathode with Field's metal (FM) encapsulation, having the ITO/NiO_x/perovskite/PCBM/AZO/FM/Pt NPs device configuration. (b) Cross-sectional scanning electron microscopy (SEM) image of the photocathode structure showing the NiO_x and perovskite layers stacked on the ITO glass substrate. (c) Thin-film X-ray diffraction pattern of triple-cation perovskite layer spin-coated on a quartz glass substrate. (d) Top view scanning transmission electron microscopy (STEM) images of spherical Pt nanoparticles grown on the surface of Field's metal by platinization. The inset shows close-up STEM image of a Pt nanoparticle. (e) Ultraviolet photoelectron spectroscopy (UPS) images of Field's metal obtained using an incident photon energy of 21.2 keV; the work function of FM is found to be −4.5 eV. (f) Corresponding energy-level diagram of the perovskite solar cell device configuration shown in (a).

melting-point metal alloy is used for the encapsulation of the perovskite layer ($CH_3NH_3PbI_3$). This device achieved an average photocurrent density of ca. −7 mA cm^{-2} at 0 V versus the reversible hydrogen electrode (RHE) and worked for 40 min under continuous illumination and about 90 min under chopped illumination.[25] In 2018, Andrei et al. demonstrated the perovskite-$BiVO_4$ photoelectrochemical (PEC) tandems for bias-free solar water splitting.[26] By employing the triple-cation (cesium formamidinium methylammonium, CsFAMA)-mixed halide perovskite as the photoabsorber and NiO_x as the hole selective layer, substantial improvements were achieved in the performance (−12.1 ± 0.3 mA cm^{-2} at 0 V versus RHE) and stability (up to 7 h) of 0.25 cm^2 photocathodes, with the corresponding solar cell devices reaching an efficiency of 13.0 ± 1.2%. Recently, Kim et al. have reported an acid-compatible triple-cation-based perovskite photocathode composed of hybrid electron transport layer, which includes phenyl-C_{61}-butyric acid methyl ester (PCBM) and atomic layer-deposited TiO_2, grown on the surface of the perovskite.[27] The photocathode under 0.5 Sun illumination has demonstrated a photocurrent density of >10 mA cm^{-2} and a photovoltage of 0.68 V assisted by proton reduction; however, in spite of conformal ALD TiO_2 encapsulation, the device still showed degradation in photocurrent density after 2 h.

Part of the limitation of the metal halide perovskite-based systems is due to the lack of appropriate charge transport layers (CTLs), as well as the limited stability of the methylammonium-based ($CH_3NH_3PbI_3$) perovskites. The poor stability of perovskite solar cells (PSCs) originates from the weakly bonded organic−inorganic halide perovskite materials,[28,29] resulting in a rapid degradation of the perovskite layer under exposure to moisture, air, or excessive heat, light, and electrical bias.[30−33] Further, the interfacial degradation of the charge transport layers and metal electrodes introduces additional degradation pathways in PSCs.[34] Some of these challenges have been addressed by optimizing the CTLs and interfaces between perovskite and metal electrodes. For instance, inverted PSC devices improve efficiency as well as stability.[35−37] Recently, PSCs with a triple-cation-based perovskite photoabsorber, using a mixture of formamidinium and methylammonium as the monovalent cation, with the addition of inorganic cesium, have shown improved air and thermal stabilities, with less sensitivity to processing conditions.[38] These triple-cation perovskites enable a more reproducible device performance and reach a stabilized

power output of ~21%.[39] In spite of promising results in solar cell performance, these triple-cation perovskite devices cannot be directly used under water,[40] and require a secondary, protective layer to stop water ingress.[25,41,26,42]

In this paper, we address the above-mentioned challenges by carefully engineering and manipulating the energy levels, with thin metal oxide films contributing toward efficient electron (Al-doped ZnO, or AZO, on PCBM)[43,41,36] and hole (nickel oxide, NiO_x)[37,44] extraction, as well as protecting the perovskite layer. A cesium formamidinium methylammonium (CsFAMA) triple-cation perovskite cell is used to provide efficient and stable light absorption and charge separation.[31,39] Field's metal (FM) alloy is used as a metal electrode for the encapsulation of the perovskite photocathode, as reported previously.[25,26] Finally, Pt catalyst nanoparticles (NPs) are synthesized on the surface of the FM coating to reduce the reaction overpotential.[25,26] The entire device stack (NiO_x/perovskite/PCBM/AZO/FM/Pt NPs) is solution-processed without any vacuum deposition step. The resulting photocathodes were submerged entirely in water and achieved a photocurrent density of ca. −14.3 mA cm^{-2} at 0 V (versus RHE), which is maintained for over 2.5 h, and decay slowly with 50% of the current density retained after 15 h. This is among the best reported for perovskite-based photoelectrodes.[25,45,46,26,42]

RESULTS AND DISCUSSION

Our proposed perovskite-based photocathode has an inverted device architecture (indium tin oxide (ITO)/NiO_x/perovskite/PCBM/AZO/FM), as depicted in Figure 1a. This is a p−i−n device structure with a NiO_x layer for hole extraction and PCBM/AZO for electron extraction. The device fabrication process and parameters are detailed in the Methods Section. Shortly, the NiO_x thin film is formed on an ITO substrate by spin coating a solution of nickel(II) nitrate hexahydrate prepared in ethylene glycol and complexed with ethylenediamine, followed by annealing steps (see Methods). A triple-cation perovskite thin film is formed by spin coating a precursor solution ($Cs_{0.05}(MA_{0.17}FA_{0.83})_{0.95}Pb(I_{0.83}Br_{0.17})_3$ or CsFAMA) on the NiO_x layer and annealing at 100 °C for 30 min in a nitrogen-filled glovebox. This results in the formation of a highly crystalline and smooth perovskite thin film, which is then coated with a layer of PCBM (20 mg mL^{-1}, chlorobenzene). An AZO thin film of thickness 37 ± 2 nm is prepared by spin coating a commercially purchased suspension of AZO nanoparticles (isopropyl alcohol (IPA) 2.5 wt %) over the PCBM film. The AZO film thickness is measured by atomic force microscopy (AFM) at the edge of the sample. AZO thin films can be fabricated by different methods; for example, Venkatesan et al.[47] spin-coated AZO coatings using a mixture of zinc acetate dihydrate in ethanol. Kumar et al.[48] showed that AZO thin films can be deposited by sputtering at different RF/(RF + DC) ratios. Ngo et al.[49] showed that ZnO thin films can also be fabricated by the spray deposition method using an airbrush.

To protect the perovskite layer from exposure to moisture or water, the devices are encapsulated with FM following a previously reported process.[25,26] Briefly, FM is molten on a hot plate at 363 K and cast to obtain a 0.5−1.0 mm thick foil. The metal foil is cooled down and cut into 12 × 7 mm^2 pieces and then placed on the perovskite device. Next, a Peltier thermoelectric element is used to melt and then solidify the FM layer (see Experimental Section for details). The edges of the devices are further sealed using a UV curing glue (NOA 63, Norland) to ensure that water does not sip through the FM and perovskite/AZO as well as FM−glass interface. Finally, Pt nanoparticles are deposited on the FM using an electroless plating process, to catalyze the hydrogen evolution. Shortly, the photoelectrode is immersed for 60 s in 10 mL of a K_2PtCl_4 aqueous solution (5.16 mM) without stirring and subsequently dipped in deionized (DI) water to wash the FM surface.

Figure 1b shows a cross-sectional SEM image of the ITO/NiO_x/perovskite stack. The size of perovskite grains ranges between 100 and 250 nm, and they are densely packed in an approximately 500 nm thick uniform film. X-ray diffraction measurements of the perovskite thin film (Figure 1c) confirm its highly crystalline nature, with a tetragonal phase matching previous reports from Saliba et al.[39,50] We note that residual PbI_2 is present (diffraction peak denoted by * in Figure 1c), in agreement with previous reports.[39,50] To protect the perovskite layer from exposure to moisture or water, which is known to dissolve the MAI and FAI cations, the devices were encapsulated with FM as described above.[25,26,51] Pt nanoparticles are deposited on the FM using an electroless plating process, through which an ohmic contact is formed between the catalytically active platinum nanoparticles and the FM, thus maintaining an efficient electron transfer to the catalyst. Scanning transmission electron microscopy (STEM) images of grown Pt nanoparticles are shown in Figure 1d, and the energy-dispersive X-ray elemental analysis of Pt nanoparticles confirms their presence on the surface of FM (for details, see Supporting Information Figures S1a−f and S2a−c).

Figure 1f shows the energy-level diagram of the ITO/NiO_x/perovskite/PCBM/AZO/FM stack, with the FM work function determined to be −4.5 eV from ultraviolet photoelectron spectroscopy (UPS) measurements performed on a polished piece of FM (Figure 1e). The work function value of FM is very close to the conduction band of the Al-doped zinc oxide (AZO) thin film (−4.3 eV).[52,53] Photoexcitation of these electrodes using a white light source (AM 1.5G filter, 100 mW cm^{-2}, 1 sun) generates electron−hole pairs in the perovskite layer; the built-in voltage developed in this p−i−n structured device due to the presence of charge specific transport layers drives the electrons and holes toward the respective metal contacts. The low exciton binding energies (<25 meV at room temperature) and long carrier diffusion lengths (~1 μm) in the perovskite semiconductor cause the photogenerated electron−hole pair to spontaneously behave like free carriers following light absorption, thus facilitating their efficient separation.[54−56,17] The work function of the AZO thin film (−4.3 eV) provides a graded band gap at the electron-selective contact with the conduction bands of perovskite, PCBM, and FM at −3.9, −4.0, and −4.5 eV, respectively. This facilitates efficient electron extraction while reducing the backtransfer of electrons into the perovskite, as well as reducing interfacial recombination, which results in a higher photocurrent in comparison to previous reports without the intermediate AZO thin film (see further). Similarly, the NiO_x hole selective thin film (work function; WF = −4.8 eV; valance band offset; E_{VB} = −5.4 eV)[44] reduces the energy barrier between the ITO (−4.7 eV) and perovskite (−5.4 eV) layers, thus forming a gradual energy landscape that enables an efficient perovskite to ITO hole extraction.

The optical absorbance spectra of the ~500 nm thick perovskite film is measured by using an integrating sphere in a standard UV−vis spectroscopy setup. The band edge from the

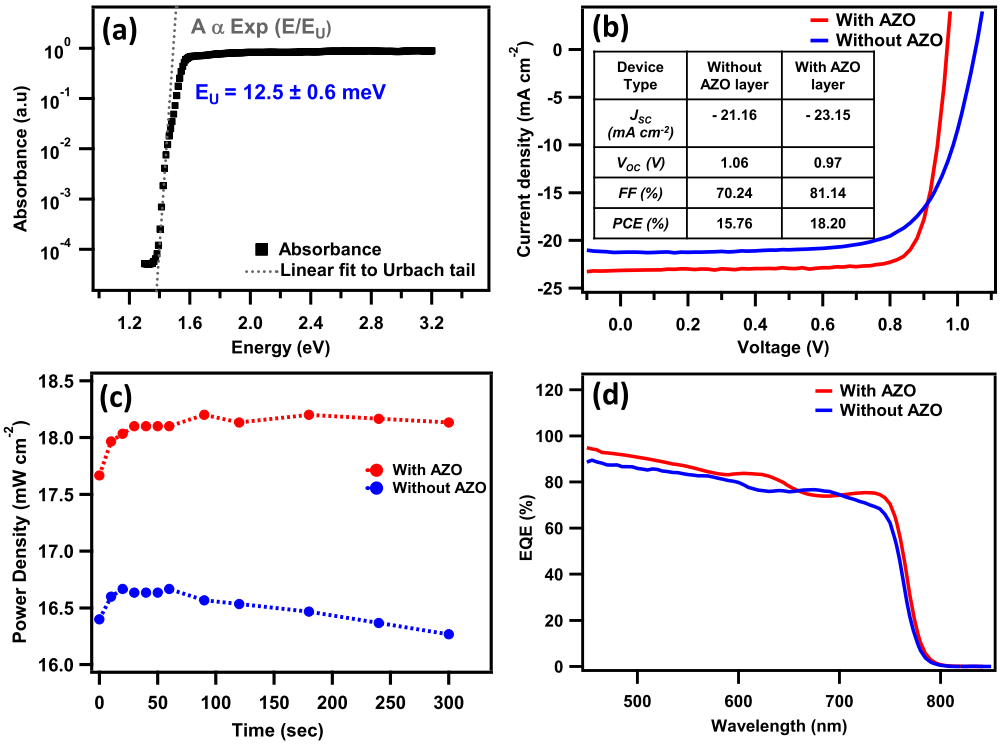


Figure 2. (a) Photothermal deflection spectroscopy (PDS) images of triple-cation perovskite thin film. (b) *IV* curve (red) of a perovskite solar cell with an AZO layer (configuration: ITO/NiO_x/perovskite/PCBM/AZO/Al) recorded under 1 sun (100 mW cm^{-2}, 100 mV s^{-1} scan rate, forward scan). An *IV* curve (blue) for a solar cell without AZO layer (configuration: ITO/NiO_x/perovskite/PCBM/Al) is added for comparison. (c) Power density variation with time for solar cell with (red dots) and without (blue dots) the AZO layer. (d) External quantum efficiency (EQE) spectra for the perovskite solar cells with and without an AZO layer.

normalized absorption spectra is found to be ~765 nm, which is in agreement with previously reported values (Supporting Information Figure S3a). The optical band gap estimated from Tauc's plot is found to be 1.62 eV (765 nm), which is similar to the triple-cation $Cs_{0.05}(MA_{0.17}FA_{0.83})_{0.95}Pb(I_{0.83}Br_{0.17})_3$ perovskite band gap reported in the literature (Supporting Information Figure S3b).[39,50] To estimate the disorder in the solution-processed CsFAMA perovskite films, they are analyzed by photothermal deflection spectroscopy (PDS).[57] PDS measurements provide a means to analyze the sub-band-gap weak absorption, thereby helping in the measurement of the exponentially falling absorption tail known as the Urbach tail. Fitting the Urbach tail gives the Urbach energy (see Figure 2a), which is a measure of the energetic disorder in the perovskite.[58] The Urbach energy of our films is 12.5 meV, which is smaller than the previously reported value of 15 meV for tri-iodide perovskite films.[59] This confirms the low levels of disorder in the triple-cation perovskite thin films demonstrated in our current work.

To evaluate the role and advantages of the thin AZO films discussed above, we fabricated solar cells with and without AZO. For simplicity and compatibility with the measurement setup, we replaced the FM with Al metal contacts for this comparison because our photovoltaic device measurement setup is only compatible with the thin-film metal contacts, not with the bulky metal contacts as obtained in the case of FM. The corresponding *IV* curves recorded under inert N_2 atmosphere are shown in Figure 2b. We masked our 4.5 mm^2 devices with an aperture of 3 mm^2 to avoid edge effects. For solar cells with an AZO layer (ITO/NiO_x/perovskite/PCBM/AZO/Al), we obtained efficiencies of up to 18.2% (red curve). By contrast, the best device without the AZO layer (ITO/NiO_x/perovskite/PCBM/Al) has an efficiency of 15.8% (blue curve). Since the Al metal contact is common in both solar cell configurations, we can confirm that the improvement in the performance of the solar cell with the AZO layer is solely due to the presence of the AZO layer. This experiment was performed to highlight the role of AZO film; however, for the final perovskite-based photocathodes, we deliberately chose FM over Al because of the ability of FM to encapsulate the photocathodes, as mentioned in the following sections.

Statistical analysis on four different devices (two each for AZO and non-AZO), with eight pixels each, confirms that the solar cells with AZO achieve higher efficiencies (average power conversion efficiency (PCE) of ~15.86%) than reference devices (PCE of ~13.90%) under the same test conditions (see Supporting Information Figure S4). This was primarily due to an increase in the fill factor from an average value of 65% (without AZO) to 79% (with AZO), along with decrease in the average series resistance from 6 Ω cm^2 (without AZO) to 3 Ω cm^2 (with AZO). These were likely due to the improved extraction of electrons from the perovskite to the metal contact, as discussed above (see Figure 1f). The slight reduction in the open-circuit voltage could be due to a decrease in effective work function at the electron-selective AZO-coated contact. Furthermore, we found that about 25% of the pixels without AZO failed, probably due to the presence of pinholes that the AZO layer seems to cover, thereby resulting in only 6% pixel failure for pixels with AZO.

The stability of the AZO-based perovskite solar cells is first examined by recording the maximum power point over time. *IV* measurements at a scan rate of 100 mV s^{-1} were repeatedly

taken at fixed intervals, showing that the intermediate AZO film increases the stability (see Figure 2c). The decay in performance of devices without intermediate AZO film could be due to degradation of the interface between the metal (Al) and the perovskite layer, since extrinsic interfacial degradation caused by metal (e.g., Ag or Al) from contacts under working conditions was previously reported.[60,61] This degradation process seems to be slowed down by the thin (15–20 nm) AZO buffer layer. Furthermore, this metal oxide layer also prohibits the degradation of the perovskite layer by reducing the halide migration out of the perovskite layer,[62] and might alleviate other degradation mechanisms as will be discussed further on when the devices are tested submerged in water.

The influence of the illumination wavelength on the performance of our devices with and without AZO coating is investigated by external quantum efficiency (EQE) measurements. The EQE spectra in Figure 2d show that for both devices, the maximum output power generation occurs in the visible spectrum of light, with a sharp cutoff edge at ~762 nm (Figure 2d), which is in accordance with the UV–vis (see Supporting Information Figure S3) and PDS (see Figure 2a) spectra of the $Cs_{0.05}(MA_{0.17}FA_{0.83})_{0.95}Pb(I_{0.83}Br_{0.17})_3$ perovskite thin films. However, for AZO-coated cells, higher photocurrents (or EQE (%)) are observed across most wavelengths. The integrated current density (J_{sc}) is −21.6 mA cm^{-2}, which is in good agreement with the average value of short-circuit current density (−21.2 mA cm^{-2}) of the AZO device obtained from *IV* measurements, averaged from two devices, with 8 pixels per device, or 16 pixels in total.

Before measuring the electrochemical performance of the perovskite photocathodes, control experiments are performed to demonstrate that the Pt nanoparticles discussed above effectively reduce the onset potential from less than −0.4 V vs RHE (ITO/FM) to around 0 V vs RHE (ITO/FM/Pt). In other words, the overpotential required for the proton reduction is minimal using the FM/Pt electrodes (see Supporting Information Figure S5).

The photoelectrochemical performance of our perovskite photocathodes is tested using a standard three-electrode configuration against a Ag/AgCl/KCl reference electrode, with a Pt mesh counter electrode. The cathodic and anodic compartments are separated through a Nafion membrane. The cyclic voltammetry (CV) scans in Figure 3a are measured at a 10 mV s^{-1} scan rate using KPi electrolyte aqueous solution (0.1 M, pH 7.0) under chopped (5 s ON and OFF) solar illumination (100 mW cm^{-2} AM 1.5G) (green curve). The sharp photocurrent response shown during the light irradiation indicates a very efficient hydrogen evolution at the perovskite/FM/Pt electrode–electrolyte interface. A high photocurrent density of −14.3 mA cm^{-2} at 0 V vs RHE is observed for the forward scan (red curve) during continuous light irradiation. To the best of our knowledge, this is one of the highest photocurrents reported so far for perovskite photocathodes fabricated entirely by solution processing.[25,45,46,26,42] A similar value of −14.2 mA cm^{-2} is observed for the reverse scan. Similarly high photocurrents are observed in several AZO-based perovskite photocathodes (see Supporting Information Figure S6a). Hysteresis is observed during forward and reverse scans in both chopped (green curve) and continuous illumination (red curve) measurements. The hysteresis is more distinct in the case of the chopped light measurements since the electrochemical potential at the FM/Pt–electrolyte interface requires more time to equilibrate. An onset potential

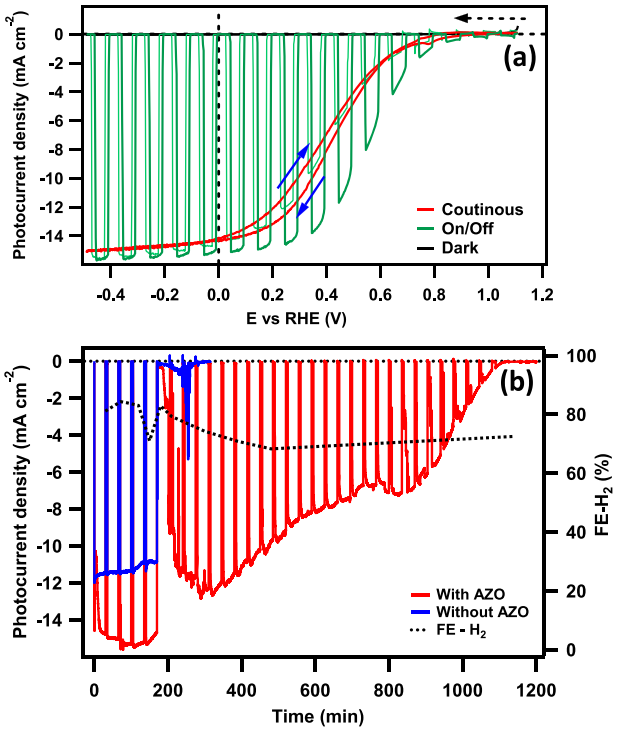


Figure 3. (a) Cyclic voltammetry of the AZO-based perovskite photocathode at a scan rate of 10 mV s^{-1}. The graph presents the scans under continuous, chopped, and without irradiation, showing little hysteresis and a greatly improved photocurrent. (b) Chronoamperometric characteristics for perovskite photocathodes with and without the AZO layer. The data are obtained at an applied potential of 0 V versus RHE. An aqueous buffer solution (0.1 M potassium phosphate, pH 7), chopped solar light irradiation (AM 1.5G, 100 mW cm^{-2}), and an inert (N_2) atmosphere at room temperature were used in both experiments. The black dots represent faradic efficiency, FE (%), of hydrogen (H_2) generation for the perovskite photocathode with an AZO layer.

of approximately 0.95 V vs RHE is achieved, which correlates to the high V_{oc} (0.97 V) of the solar cell with an AZO layer, suggesting a very small energy loss at the perovskite/FM interface. In comparison, cyclic voltammograms of perovskite photocathodes without AZO coating tested under the same conditions showed a lower photocurrent density of approximately −12 mA cm^{-2} at 0 V vs RHE (Supporting Information Figure S6b).

Next, the stability of the AZO-based perovskite photocathodes is evaluated using chronoamperometry in the same three-electrode configuration. To monitor changes in the dark currents, the light is chopped off for 5 min after every 30 min of exposure. A high absolute photocurrent density of more than 14 mA cm^{-2} is maintained for almost 3 h with the AZO-coated perovskite photocathodes (red curve, Figure 3b). The photocurrent shows a slow initial rise upon illumination, which is probably due to the migration of halides, decreasing the trap state density, similar to the photoinduced effects reported for perovskite photovoltaic devices.[30,63,64,66] A dip in photocurrent density is observed after ~2.5 h, which first rectifies and then continues to decay slowly, but retains half of the initial photocurrent intensity for about 15 h. We attribute this sudden decay in photocurrent to partial damage of the cell (active pixel area) caused by the exposure of cell to the electrolyte as well as light. While stress under operation may cause degradation of

the electrical contacts and pinholes in the device architecture leading to this unusual behavior, it seems that the AZO layer is able to provide enough spatial separation between the contacts to avoid an irreversible shorting of the device, enabling a continuous operation even under mild damage. CV scans of photocathodes without AZO coating are shown in Supporting Information Figure S6b, and their chronoamperometry (blue curve, Figure 3b) shows a lower photocurrent (−11.8 mA cm^{-2}), which is consistent with the measurements on non-AZO perovskite solar cells reported above (see Figures 2b−d and S4). Further, the perovskite photocathode without AZO stopped working after 2.5 h of light irradiation. It must be noted that in contrast to a previous work,[25] employing an $MAPbI_3$ perovskite with a hydrophilic poly(3,4-ethylenedioxythiophene):polystyrene sulfonate selective layer, the non-AZO devices reported here demonstrate high photocurrents under continuous light exposure, just due to highly crystalline triple-cation-based perovskite in combination with a robust NiO_x hole transport layer.

CONCLUSIONS

We present a triple-cation cesium formamidinium methylammonium (CsFAMA)-based metal halide perovskite photocathode for solar fuel generation. The photocurrent and stability of these electrodes are enhanced by solution-processed AZO and NiO_x layers. In particular, AZO as an electron transport layer showed an increase in photocurrent density of ∼20% along with a 5-fold extension of the device lifetime, which reached up to 18 h before complete failure. This AZO coating also covers pinholes, and as a result, the number of failed pixels reduced from 25 to 6%. Finally, the photocathodes are fabricated using low-cost and scalable methods that have promise to become compatible with standard solution processes, and therefore provide a significant contribution toward the efficient fabrication of solar fuel generation devices.

METHODS

Perovskite Solar Cell Fabrication. Patterned ITO glass substrates are cleaned by ultrasonication in acetone and *iso*-propanol (15 min each), followed by an oxygen plasma treatment for 10 min using a Diener Plasma etcher. A NiO_x thin film is spin-coated on ITO substrates following a previously reported procedure,[44] where a nickel oxide precursor solution is prepared by dissolving nickel(II) nitrate hexahydrate ($Ni(NO_3)_2{\cdot}6H_2O$, 1 M) (Sigma-Aldrich) in ethylene glycol with 1 M ethylenediamine (Aldrich). The solution is spin-cast onto ITO glass substrate at a spin speed of 5000 rpm for 45 s. The substrates are then annealed in ambient air at 100 °C for 30 min, then 300 °C for 60 min, resulting in a NiO_x film of ∼50 nm thickness. The NiO_x-coated ITO substrates were then transferred inside a N_2-filled glovebox for completing the device fabrication to avoid moisture accumulation on the surface. The triple-cation perovskite precursor solution is prepared by adding CsI, FAI, and MABr in stochiometric ratio of PbI_2 and $PbBr_2$ in dimethylformamide/dimethyl sulfoxide (DMF/DMSO), as demonstrated by Saliba et al.[39] In short, FAI (1 M), PbI_2 (1.1 M), MABr (0.2 M), and $PbBr_2$ (0.2 M) are dissolved in anhydrous DMF/DMSO 4:1 (v/v). We note that this composition contains a lead excess as reported elsewhere.[38,65] Then CsI, predissolved as a 1.5 M stock solution in DMSO, was added to the mixed perovskite precursor to achieve the desired triple-cation composition with generic form of $Cs_{0.05}(MA_{0.17}FA_{0.83})_{0.95}Pb(I_{0.83}Br_{0.17})_3$. The perovskite solution was spin-coated in a two-step program, at 1000 and 6000 rpm for 10 and 20 s, respectively. During the second step, 75 μL of chloroform as antisolvent was poured on the spinning substrate 5 s prior to the end of the program. Films with Cs-containing perovskite turned dark immediately after spin coating. The substrates were then annealed (usually at 100 °C) for 1 h in a nitrogen-filled glovebox. The annealing step converted the spin-coated films into highly crystalline perovskite films. After cooling, PCBM is spin-coated (step 1: 2000 rpm, 40 s; step 2: 3000 rpm, 10 s) on top of the annealed perovskite film using a PCBM solution (20 mg/mL) in chlorobenzene.

AZO Layer. The Al-doped zinc oxide Al/ZnO (3.15 mol % Al) (AZO) thin film is prepared by using a commercially purchased suspension of AZO nanoparticles (IPA 2.5 wt %) with average particle size of 12 nm (Nanograde product number: 8045). AZO solution (as received) is dynamically spin-coated at 5000 rpm for 30 s on PCBM film to obtain a thin layer (thickness: 37 ± 2 nm) of AZO. Film thickness is measured by performing atomic force microscopy (AFM) to measure a step edge made on the film. These measurements were made using a Bruker Multimode 8. Silicon tips were used with a cantilever resonant frequency of 300 kHz. A set of perovskite solar cells are also fabricated without the AZO layer for comparing the device performance. For solar cell *IV* curve measurements, a 95−100 nm thick Al metal contact is thermally evaporated onto the AZO film under high vacuum. The pixel active area is kept fixed at 3.0 mm^2 by using a shadow mask. Similar-thickness Al metal contacts are used in non-AZO-based perovskite solar cells.

Field's Metal Electrode and Platinization. An eutectic alloy of In, Sn, and Bi (Field's metal), with weight % ratio of Bi/In/Sn = 32.5:51:16.5, is used as both metallic contact and encapsulation layer on top of the AZO film. The perovskite photocathodes (active area ≈ 0.16 cm^2) are fabricated onto 12 × 12 mm^2 etched ITO glass substrates. All other layers on ITO, including NiO_x/perovskite/PCBM/AZO, are fabricated in a similar way as discussed for the solar cells. The protective FM layer is encapsulated on the top of AZO layer by using earlier reported methods.[26] In short, Field's metal piece is melted on a hot plate at 363 K (90 °C) to obtain a 0.5−1.0 mm thick foil by spreading. After solidifying, the metal foil is cut into 12 × 7 mm^2 pieces, which are gently placed on the perovskite devices in such a way that they cover the pixel area completely. Next, the pieces of FM are briefly molten onto the devices, by applying 2.4 A for 30 s to a Peltier thermoelectric element using an IviumStat potentiostat, and then solidified by applying −2.4 A for 30 s. The edges of the devices are further sealed using a UV curing glue (NOA 63, Norland) to make sure that water should not sieve in through the FM and perovskite/AZO interface. The Pt catalyst nanoparticles are grown on FM by dipping the encapsulated device, attached to the stainless steel holder, in a K_2PtCl_4 (98%, Sigma, pH 1.2) solution for 60 s, without stirring. The devices are subsequently dipped into DI water to rinse the excess of K_2PtCl_4. The ITO glass back side of the device is cleaned by using a cotton swipe before performing photoelectrochemical measurements.

Solar Cell Measurements. The ITO/NiO_x/perovskite/PCBM/AZO/Al device configuration is maintained for solar cell measurements. The AZO-free solar cells are also characterized in the same way. An ABET solar simulator, corrected for spectral mismatch to give a spectrum matching AM 1.5G over the wavelength range absorbed by the perovskite cells, is used for the illumination and *IV* characteristics were recorded by using a Keithley source meter (model no. 2450).

Photoelectrochemical Measurements. Photoelectrochemical (PEC) measurements were carried out on an electrochemical workstation (Ivium CompactStat), under inert (N_2, with 2% CH_4) atmosphere, at room temperature. A conventional three-electrode configuration was used with the perovskite photocathode, Pt mesh, and Ag/AgCl/KCl (sat) acting as a working, counter, and reference electrodes, respectively, in an aqueous potassium phosphate buffer [K_2HPO_4 (107 g) and KH_2PO_4 (52 g) in H_2O (1 L), adjusted to pH 7 using H_2SO_4]. The measurements were done using cyclic voltammetry (CV) scans for a potential range of 1.1 V to −0.5 V vs RHE at a scan rate of 10 mV s^{-1} (0.1 M KPi electrolyte aqueous solution at pH 7.0). The potential conversion from Ag/AgCl to RHE is done by using the following relationship

$$E\ (\text{Vversus RHE}) = E\ (\text{Vversus Ag/AgCl}) + (0.059 \times \text{pH}) + 0.197$$

Therefore, for pH 7.0, 0 V vs RHE = −0.610 V vs Ag/AgCl.

The two compartments of the glass PEC cell were separated by a Nafion ion-selective membrane. The evolved H_2 was quantified by manually injecting 100 μL of the gaseous headspace into a Shimadzu GC-2010 Plus gas chromatograph (GC). The faradic efficiency (FE) was calculated from the H_2 amount and the corresponding total charge at a given time.

■ ASSOCIATED CONTENT

STEM images and EDAX of Field's metal before and after platinization, optical absorption spectra and Tauc's plot of cesium formamidinium methylammonium (CsFAMA) triple-cation-lead halide perovskite thin film, statistical data on power conversion efficiency (PCE %) measurements, cyclic voltammetry for control experiments on ITO/FM and ITO/FM/Pt electrodes, and cyclic voltammetry of the perovskite photocathodes (PDF)

■ AUTHOR INFORMATION

Corresponding Authors

*E-mail: sahmad28@jmi.ac.in (S.A.).
*E-mail: mfld2@cam.ac.uk (M.D.V.).

ORCID

Shahab Ahmad: 0000-0002-7846-4804
Aditya Sadhanala: 0000-0003-2832-4894
Robert L. Z. Hoye: 0000-0002-7675-0065
Richard Friend: 0000-0001-6565-6308
Michael De Volder: 0000-0003-1955-2270

Present Address

[#]Department of Materials Science and Metallurgy, University of Cambridge, 27 Charles Babbage Road, Cambridge CB3 0FS, United Kingdom (R.L.Z.H.). Clarendon Laboratory, Department of Physics, University of Oxford, Parks Road, Oxford OX1 3PU, United Kingdom (A.S.).

Notes

The authors declare no competing financial interest.

■ ACKNOWLEDGMENTS

S.A. and M.D.V. acknowledge the financial support from an ERC Starting Grant (337739 HIENA) and DST-UKIERI (DST/INT/UK/P-167/2017). S.A. acknowledges the financial support from UGC Start-Up (30-422/2018 BSR) Research Grants. R.L.Z.H. acknowledges the support from the Royal Academy of Engineering under the Research Fellowship scheme (No. RF/201718/17101), as well as the support from Magdalene College, Cambridge. V.A. is grateful for the financial support from the Cambridge Trusts (Vice-Chancellor's Award) and the Winton Programme for the Physics of Sustainability. M.H.M acknowledges the support from EPSRC Cambridge NanoDTC, EP/G037221/1. J.R. acknowledge the financial support by the Research Foundation—Flanders. A.S. and R.F. acknowledge support from the UKRI Global Challenge Research Fund project, SUNRISE (EP/P032591/1), Winton Programme for the Physics of Sustainability (University of Cambridge), and Indo-UK joint project (APEX Phase II). The authors thank Prof Erwin Reisner for his support in this study and providing feedback on the manuscript.

■ REFERENCES

(1) Ciamician, G. The Photochemistry Of The Future. *Science* **1912**, *36*, 385−394.

(2) Ryabchuk, V.; Kuznetsov, V.; Emeline, A.; Artem'ev, Y.; Kataeva, G.; Horikoshi, S.; Serpone, N. Water Will Be the Coal of the Future-The Untamed Dream of Jules Verne for a Solar Fuel. *Molecules* **2016**, *21*, 1638−1658.

(3) Venturi, M.; Balzani, V.; Gandolfi, M. T. In *Fuels From Solar Energy. A Dream Of Giacomo Ciamician, The Father Of Photochemistry*, American Solar Energy Society Proceedings 2005, August 6−12; Solar World Congress: Orlando, Florida.

(4) Fujishima, A.; Honda, K. Electrochemical Photolysis of Water at a Semiconductor Electrode. *Nature* **1972**, *238*, 37−38.

(5) Walter, M. G.; Warren, E. L.; McKone, J. R.; Boettcher, S. W.; Mi, Q.; Santori, E. A.; Lewis, N. S. Solar Water Splitting Cells. *Chem. Rev.* **2010**, *110*, 6446−6473.

(6) Tachibana, Y.; Vayssieres, L.; Durrant, J. R. Artificial Photosynthesis for Solar Water-Splitting. *Nat. Photonics* **2012**, *6*, 511−518.

(7) Nguyen, P. D.; Duong, T. M.; Tran, P. D. Current Progress and Challenges in Engineering Viable Artificial Leaf for Solar Water Splitting. *J. Sci.: Adv. Mater. Devices* **2017**, *2*, 399−417.

(8) Kudo, A.; Miseki, Y. Heterogeneous hydrogen evolution. Shortly, theMaterials for Water Splitting. *Chem. Soc. Rev.* **2009**, *38*, 253−278.

(9) Young, J. L.; Steiner, M. A.; Döscher, H.; France, R. M.; Turner, J. A.; Deutsch, T. G. Direct Solar-to-Hydrogen Conversion via Inverted Metamorphic Multi-Junction Semiconductor Architectures. *Nat. Energy* **2017**, *2*, No. 17028.

(10) Walczak, K. A.; Segev, G.; Larson, D. M.; Beeman, J. W.; Houle, F. A.; Sharp, I. D. Hybrid Composite Coatings for Durable and Efficient Solar Hydrogen Generation under Diverse Operating Conditions. *Adv. Energy Mater.* **2017**, *7*, No. 1602791.

(11) Roger, I.; Shipman, M. A.; Symes, M. D. Earth-Abundant Catalysts for Electrochemical and Photoelectrochemical Water Splitting. *Nat. Rev. Chem.* **2017**, *1*, No. 0003.

(12) Suen, N.-T.; Hung, S.-F.; Quan, Q.; Zhang, N.; Xu, Y.-J.; Chen, H. M. Electrocatalysis for the Oxygen Evolution Reaction: Recent Development and Future Perspectives. *Chem. Soc. Rev.* **2017**, *46*, 337−365.

(13) Hunter, B. M.; Gray, H. B.; Müller, A. M. Earth-Abundant Heterogeneous Water Oxidation Catalysts. *Chem. Rev.* **2016**, *116*, 14120−14136.

(14) Sun, K.; Liu, R.; Chen, Y.; Verlage, E.; Lewis, N. S.; Xiang, C. Solar-Driven Water Splitting: A Stabilized, Intrinsically Safe, 10% Efficient, Solar-Driven Water-Splitting Cell Incorporating Earth-Abundant Electrocatalysts with Steady-State PH Gradients and Product Separation Enabled by a Bipolar Membrane. *Adv. Energy Mater.* **2016**, *6*, No. 1600379.

(15) Luo, J.; Vermaas, D. A.; Bi, D.; Hagfeldt, A.; Smith, W. A.; Grätzel, M. Bipolar Membrane-Assisted Solar Water Splitting in Optimal PH. *Adv. Energy Mater.* **2016**, *6*, No. 1600100.

(16) Lu, H.; Andrei, V.; Jenkinson, K. J.; Regoutz, A.; Li, N.; Creissen, C. E.; Wheatley, A. E. H.; Hao, H.; Reisner, E.; Wright, D. S.; Pike, S. D. Single-Source Bismuth (Transition Metal) Polyoxovanadate Precursors for the Scalable Synthesis of Doped $BiVO_4$ Photoanodes. *Adv. Mater.* **2018**, *30*, No. 1804033.

(17) Stranks, S. D.; Eperon, G. E.; Grancini, G.; Menelaou, C.; Alcocer, M. J. P.; Leijtens, T.; Herz, L. M.; Petrozza, A.; Snaith, H. J. Electron-Hole Diffusion Lengths Exceeding 1 Micrometer in an Organometal Trihalide Perovskite Absorber. *Science* **2013**, *342*, 341−344.

(18) Li, Y.; Yan, W.; Li, Y.; Wang, S.; Wang, W.; Bian, Z.; Xiao, L.; Gong, Q. Direct Observation of Long Electron-Hole Diffusion Distance in $CH_3NH_3PbI_3$ Perovskite Thin Film. *Sci. Rep.* **2015**, *5*, No. 14485.

(19) Poindexter, J. R.; Hoye, R. L. Z.; Nienhaus, L.; Kurchin, R. C.; Morishige, A. E.; Looney, E. E.; Osherov, A.; Correa-Baena, J.-P.; Lai, B.; Bulović, V.; Stevanovic, V.; Bawendi, M. G.; Buonassisi, T. High Tolerance to Iron Contamination in Lead Halide Perovskite Solar Cells. *ACS Nano* **2017**, *11*, 7101−7109.
(20) Ahmad, S.; George, C.; Beesley, D. J.; Baumberg, J. J.; De Volder, M. Photo-Rechargeable Organo-Halide Perovskite Batteries. *Nano Lett.* **2018**, *18*, 1856−1862.
(21) Ahmad, S.; Hanmandlu, C.; Kanaujia, P. K.; Prakash, G. V. Direct Deposition Strategy for Highly Ordered Inorganic Organic Perovskite Thin Films and Their Optoelectronic Applications. *Opt. Mater. Express* **2014**, *4*, 1313−1323.
(22) Da, P.; Cha, M.; Sun, L.; Wu, Y.; Wang, Z.-S.; Zheng, G. High-Performance Perovskite Photoanode Enabled by Ni Passivation and Catalysis. *Nano Lett.* **2015**, *15*, 3452−3457.
(23) Hoang, M. T.; Pham, N. D.; Han, J. H.; Gardner, J. M.; Oh, I. Integrated Photoelectrolysis of Water Implemented On Organic Metal Halide Perovskite Photoelectrode. *ACS Appl. Mater. Interfaces* **2016**, *8*, 11904−11909.
(24) Wang, C.; Yang, S.; Chen, X.; Wen, T.; Yang, H. G. Surface-Functionalized Perovskite Films for Stable Photoelectrochemical Water Splitting. *J. Mater. Chem. A* **2017**, *5*, 910−913.
(25) Crespo-Quesada, M.; Pazos-Outón, L. M.; Warnan, J.; Kuehnel, M. F.; Friend, R. H.; Reisner, E. Metal-Encapsulated Organolead Halide Perovskite Photocathode for Solar-Driven Hydrogen Evolution in Water. *Nat. Commun.* **2016**, *7*, No. 12555.
(26) Andrei, V.; Hoye, R. L. Z.; Crespo-Quesada, M.; Bajada, M.; Ahmad, S.; De Volder, M.; Friend, R.; Reisner, E. Scalable Triple Cation Mixed Halide Perovskite-$BiVO_4$ Tandems for Bias-Free Water Splitting. *Adv. Energy Mater* **2018**, No. 1801403.
(27) Kim, I. S.; Pellin, M. J.; Martinson, A. B. F. Acid-Compatible Halide Perovskite Photocathodes Utilizing Atomic Layer Deposited TiO_2 for Solar-Driven Hydrogen Evolution. *ACS Energy Lett.* **2019**, *4*, 293−298.
(28) Kim, H.-S.; Seo, J.-Y.; Park, N.-G. Material and Device Stability in Perovskite Solar Cells. *ChemSusChem* **2016**, *9*, 2528−2540.
(29) Walsh, A. Principles of Chemical Bonding and Band Gap Engineering in Hybrid Organic−Inorganic Halide Perovskites. *J. Phys. Chem. C* **2015**, *119*, 5755−5760.
(30) Hoke, E. T.; Slotcavage, D. J.; Dohner, E. R.; Bowring, A. R.; Karunadasa, H. I.; McGehee, M. D. Reversible Photo-Induced Trap Formation in Mixed-Halide Hybrid Perovskites for Photovoltaics. *Chem. Sci.* **2015**, *6*, 613−617.
(31) Habisreutinger, S. N.; McMeekin, D. P.; Snaith, H. J.; Nicholas, R. J. Research Update: Strategies for Improving the Stability of Perovskite Solar Cells. *APL Mater.* **2016**, *4*, No. 091503.
(32) Yang, J.; Siempelkamp, B. D.; Liu, D.; Kelly, T. L. Investigation of $CH_3NH_3PbI_3$ Degradation Rates and Mechanisms in Controlled Humidity Environments Using in Situ Techniques. *ACS Nano* **2015**, *9*, 1955−1963.
(33) Conings, B.; Drijkoningen, J.; Gauquelin, N.; Babayigit, A.; D'Haen, J.; D'Olieslaeger, L.; Ethirajan, A.; Verbeeck, J.; Manca, J.; Mosconi, E.; De Angelis, F.; Boyen, H. Intrinsic Thermal Instability of Methylammonium Lead Trihalide Perovskite. *Adv. Energy Mater.* **2015**, *5*, No. 1500477.
(34) Wang, D.; Wright, M.; Elumalai, N. K.; Uddin, A. Stability of Perovskite Solar Cells. *Sol. Energy Mater. Sol. Cells* **2016**, *147*, 255−275.
(35) Chen, W.; Wu, Y.; Yue, Y.; Liu, J.; Zhang, W.; Yang, X.; Chen, H.; Bi, E.; Ashraful, I.; Grätzel, M.; Liyuan, H. Efficient and Stable Large-Area Perovskite Solar Cells with Inorganic Charge Extraction Layers. *Science* **2015**, *350*, 944−948.
(36) Brinkmann, K. O.; Zhao, J.; Pourdavoud, N.; Becker, T.; Hu, T.; Olthof, S.; Meerholz, K.; Hoffmann, L.; Gahlmann, T.; Heiderhoff, R.; Oszajca, M. F.; Luechinger, N. A.; Rogalla, D.; Chen, Y.; Cheng, B.; Riedl, T. Suppressed Decomposition of Organometal Halide Perovskites by Impermeable Electron-Extraction Layers in Inverted Solar Cells. *Nat. Commun.* **2017**, *8*, No. 13938.
(37) You, J.; Meng, L.; Song, T.-B.; Guo, T.-F.; Yang, Y. M.; Chang, W.-H.; Hong, Z.; Chen, H.; Zhou, H.; Chen, Q.; Liu, Y.; Marco, N. De; Yang, Y. Improved Air Stability of Perovskite Solar Cells via Solution-Processed Metal Oxide Transport Layers. *Nat. Nanotechnol.* **2016**, *11*, 75−81.
(38) Jacobsson, T. J.; Svanström, S.; Andrei, V.; Rivett, J. P. H.; Kornienko, N.; Philippe, B.; Cappel, U. B.; Rensmo, H.; Deschler, F.; Boschloo, G. Extending the Compositional Space of Mixed Lead Halide Perovskites by Cs, Rb, K, and Na Doping. *J. Phys. Chem. C* **2018**, *122*, 13548−13557.
(39) Saliba, M.; Matsui, T.; Seo, J.-Y.; Domanski, K.; Correa-Baena, J.-P.; Nazeeruddin, M. K.; Zakeeruddin, S. M.; Tress, W.; Abate, A.; Hagfeldt, A.; Grätzel, M. Cesium-Containing Triple Cation Perovskite Solar Cells: Improved Stability, Reproducibility and High Efficiency. *Energy Environ. Sci.* **2016**, *9*, 1989−1997.
(40) Sun, Y.; Peng, J.; Chen, Y.; Yao, Y.; Liang, Z. Triple-Cation Mixed-Halide Perovskites: Towards Efficient, Annealing-Free and Air-Stable Solar Cells Enabled by $Pb(SCN)_2$ Additive. *Sci. Rep.* **2017**, *7*, No. 46193.
(41) Seo, S.; Jeong, S.; Bae, C.; Park, N.-G.; Shin, H. Perovskite Solar Cells with Inorganic Electron- and Hole-Transport Layers Exhibiting Long-Term (≈500 h) Stability at 85 °C under Continuous 1 Sun Illumination in Ambient Air. *Adv. Mater.* **2018**, *30*, No. 1801010.
(42) Zhang, H.; Yang, Z.; Yu, W.; Wang, H.; Ma, W.; Zong, X.; Li, C. A Sandwich-Like Organolead Halide Perovskite Photocathode for Efficient and Durable Photoelectrochemical Hydrogen Evolution in Water. *Adv. Energy Mater.* **2018**, *8*, No. 1800795.
(43) Zhang, L. Q.; Zhang, X. W.; Yin, Z. G.; Jiang, Q.; Liu, X.; Meng, J. H.; Zhao, Y. J.; Wang, H. L. Highly Efficient and Stable Planar Heterojunction Perovskite Solar Cells via a Low Temperature Solution Process. *J. Mater. Chem. A* **2015**, *3*, 12133−12138.
(44) Hoye, R. L. Z.; Lee, L. C.; Kurchin, R. C.; Huq, T. N.; Zhang, K. H. L.; Sponseller, M.; Nienhaus, L.; Brandt, R. E.; Jean, J.; Polizzotti, J. A.; Kursumović, A.; Bawendi, M. G.; Bulović, V.; Stevanović, V.; Buonassisi, T.; MacManus-Driscoll, J. L. Strongly Enhanced Photovoltaic Performance and Defect Physics of Air-Stable Bismuth Oxyiodide (BiOI). *Adv. Mater.* **2017**, *29*, No. 1702176.
(45) Luo, J.; Im, J.-H.; Mayer, M. T.; Schreier, M.; Nazeeruddin, M. K.; Park, N.-G.; Tilley, S. D.; Fan, H. J.; Gratzel, M. Water Photolysis at 12.3% Efficiency via Perovskite Photovoltaics and Earth-Abundant Catalysts. *Science* **2014**, *345*, 1593−1596.
(46) Gurudayal; Sabba, D.; Kumar, M. H.; Wong, L. H.; Barber, J.; Grätzel, M.; Mathews, N. Perovskite−Hematite Tandem Cells for Efficient Overall Solar Driven Water Splitting. *Nano Lett.* **2015**, *15*, 3833−3839.
(47) Venkatesan, S.; Ngo, E.; Khatiwada, D.; Zhang, C.; Qiao, Q. Enhanced Lifetime of Polymer Solar Cells by Surface Passivation of Metal Oxide Buffer Layers. *ACS Appl. Mater. Interfaces* **2015**, *7*, 16093−16100.
(48) Kumar, N.; Dubey, A.; Bahrami, B.; Venkatesan, S.; Qiao, Q.; Kumar, M. Origin of High Carrier Mobility and Low Residual Stress in RF Superimposed DC Sputtered Al Doped ZnO Thin Film for next Generation Flexible Devices. *Appl. Surf. Sci.* **2018**, *436*, 477−485.
(49) Ngo, E.; Venkatesan, S.; Galipeau, D.; Qiao, Q. Polymer Photovoltaic Performance and Degradation on Spray and Spin Coated Electron Transport Layer and Active Layer. *IEEE Trans. Electron Devices* **2013**, *60*, 2372−2378.
(50) Saliba, M.; Matsui, T.; Domanski, K.; Seo, J.-Y.; Ummadisingu, A.; Zakeeruddin, S. M.; Correa-Baena, J.-P.; Tress, W. R.; Abate, A.; Hagfeldt, A.; Grätzel, M. Incorporation of Rubidium Cations into Perovskite Solar Cells Improves Photovoltaic Performance. *Science* **2016**, *354*, 206−209.
(51) Crespo-Quesada, M.; Reisner, E. Emerging Approaches to Stabilise Photocorrodible Electrodes and Catalysts for Solar Fuel Applications. *Energy Environ. Sci.* **2017**, *10*, 1116−1127.
(52) Kim, H.-M.; Youn, J.-H.; Seo, G.-J.; Jang, J. Inverted Quantum-Dot Light-Emitting Diodes with Solution-Processed Aluminium−Zinc Oxide as a Cathode Buffer. *J. Mater. Chem. C* **2013**, *1*, 1567−1573.

(53) Peng, L.; Tang, J.; Zhu, M. Recent Development in Colloidal Quantum Dots Photovoltaics. *Front. Optoelectron.* **2012**, *5*, 358−370.
(54) Miyata, A.; Mitioglu, A.; Plochocka, P.; Portugall, O.; Wang, J. T.-W.; Stranks, S. D.; Snaith, H. J.; Nicholas, R. J. Direct Measurement of the Exciton Binding Energy and Effective Masses for Charge Carriers in Organic−Inorganic Tri-Halide Perovskites. *Nat. Phys.* **2015**, *11*, 582−587.
(55) Galkowski, K.; Mitioglu, A.; Miyata, A.; Plochocka, P.; Portugall, O.; Eperon, G. E.; Wang, J. T.-W.; Stergiopoulos, T.; Stranks, S. D.; Snaith, H. J.; Nicholas, R. J. Determination of the Exciton Binding Energy and Effective Masses for Methylammonium and Formamidinium Lead Tri-Halide Perovskite Semiconductors. *Energy Environ. Sci.* **2016**, *9*, 962−970.
(56) Yang, Z.; Surrente, A.; Galkowski, K.; Bruyant, N.; Maude, D. K.; Haghighirad, A. A.; Snaith, H. J.; Plochocka, P.; Nicholas, R. J. Unraveling the Exciton Binding Energy and the Dielectric Constant in Single-Crystal Methylammonium Lead Triiodide Perovskite. *J. Phys. Chem. Lett.* **2017**, *8*, 1851−1855.
(57) Jackson, W. B.; Amer, N. M.; Boccara, A. C.; Fournier, D. Photothermal Deflection Spectroscopy and Detection. *Appl. Opt.* **1981**, *20*, 1333.
(58) Zhao, B.; Abdi-Jalebi, M.; Tabachnyk, M.; Glass, H.; Kamboj, V. S.; Nie, W.; Pearson, A. J.; Puttisong, Y.; Gödel, K. C.; Beere, H. E.; Ritchie, D. A.; Mohite, A. D.; Dutton, S. E.; Friend, R. H.; Sadhanala, A. High Open-Circuit Voltages in Tin-Rich Low-Bandgap Perovskite-Based Planar Heterojunction Photovoltaics. *Adv. Mater.* **2017**, *29*, No. 1604744.
(59) Sadhanala, A.; Deschler, F.; Thomas, T. H.; Dutton, S. E.; Goedel, K. C.; Hanusch, F. C.; Lai, M. L.; Steiner, U.; Bein, T.; Docampo, P.; Cahen, D.; Friend, R. H. Preparation of Single-Phase Films of $CH_3NH_3Pb(I_{1-x}Br_x)_3$ with Sharp Optical Band Edges. *J. Phys. Chem. Lett.* **2014**, *5*, 2501−2505.
(60) Domanski, K.; Correa-Baena, J.-P.; Mine, N.; Nazeeruddin, M. K.; Abate, A.; Saliba, M.; Tress, W.; Hagfeldt, A.; Grätzel, M. Not All That Glitters Is Gold: Metal-Migration-Induced Degradation in Perovskite Solar Cells. *ACS Nano* **2016**, *10*, 6306−6314.
(61) Guerrero, A.; You, J.; Aranda, C.; Kang, Y. S.; Garcia-Belmonte, G.; Zhou, H.; Bisquert, J.; Yang, Y. Interfacial Degradation of Planar Lead Halide Perovskite Solar Cells. *ACS Nano* **2016**, *10*, 218−224.
(62) Kaltenbrunner, M.; Adam, G.; Głowacki, E. D.; Drack, M.; Schwödiauer, R.; Leonat, L.; Apaydin, D. H.; Groiss, H.; Scharber, M. C.; White, M. S.; Sariciftci, N. S.; Bauer, S. Flexible High Power-per-Weight Perovskite Solar Cells with Chromium Oxide−Metal Contacts for Improved Stability in Air. *Nat. Mater.* **2015**, *14*, 1032−1039.
(63) deQuilettes, D. W.; Zhang, W.; Burlakov, V. M.; Graham, D. J.; Leijtens, T.; Osherov, A.; Bulović, V.; Snaith, H. J.; Ginger, D. S.; Stranks, S. D. Photo-Induced Halide Redistribution in Organic−Inorganic Perovskite Films. *Nat. Commun.* **2016**, *7*, No. 11683.
(64) Barker, A. J.; Sadhanala, A.; Deschler, F.; Gandini, M.; Senanayak, S. P.; Pearce, P. M.; Mosconi, E.; Pearson, A. J.; Wu, Y.; Srimath Kandada, A. R.; Leijtens, T.; Angelis, F. De; Dutton, S. E.; Petrozza, A.; Friend, R. H. Defect-Assisted Photoinduced Halide Segregation in Mixed-Halide Perovskite Thin Films. *ACS Energy Lett.* **2017**, *2*, 1416−1424.
(65) Jacobsson, T. J.; Correa-Baena, J.-P.; Halvani Anaraki, E.; Philippe, B.; Stranks, S. D.; Bouduban, M. E. F.; Tress, W.; Schenk, K.; Teuscher, J.; Moser, J.-E.; Rensmo, H.; Hagfeldt, A. Unreacted PbI_2 as a Double-Edged Sword for Enhancing the Performance of Perovskite Solar Cells. *J. Am. Chem. Soc.* **2016**, *138*, 10331−10343.
(66) Ahmad, S.; Kanaujia, P. K.; Beeson, H. J.; Abate, A.; Deschler, F.; Credgington, D.; Steiner, U.; Prakash, G. V.; Baumberg, J. Strong Photocurrent from Two-Dimensional Excitons in Solution-Processed Stacked Perovskite Semiconductor Sheets. *ACS Appl. Mater. Interfaces* **2015**, *7*, 25227−25236.